Redistribution of caveolae during mitosis

Emmanuel Boucrot[1,*], Mark T. Howes[2], Tomas Kirchhausen[1,‡] and Robert G. Parton[2,‡]

[1]Department of Cell Biology and Immune Disease Institute, Harvard Medical School, Boston, MA 02115, USA
[2]The University of Queensland, Institute for Molecular Bioscience and Centre for Microscopy and Microanalysis, Queensland 4072, Brisbane, Australia

*Present address: MRC-Laboratory of Molecular Biology, Hills Road, Cambridge CB2 0QH, UK
‡Authors for correspondence (kirchhausen@crystal.harvard.edu; r.parton@imb.uq.edu.au)

Accepted 10 February 2011
Journal of Cell Science 124, 1965-1972

doi:10.1242/jcs.076570

Summary

Caveolae form a specialized platform within the plasma membrane that is crucial for an array of important biological functions, ranging from signaling to endocytosis. Using total internal reflection fluorescence (TIRF) and 3D fast spinning-disk confocal imaging to follow caveola dynamics for extended periods, and electron microscopy to obtain high resolution snapshots, we found that the vast majority of caveolae are dynamic with lifetimes ranging from a few seconds to several minutes. Use of these methods revealed a change in the dynamics and localization of caveolae during mitosis. During interphase, the equilibrium between the arrival and departure of caveolae from the cell surface maintains the steady-state distribution of caveolin-1 (Cav1) at the plasma membrane. During mitosis, increased dynamics coupled to an imbalance between the arrival and departure of caveolae from the cell surface induces a redistribution of Cav1 from the plasma membrane to intracellular compartments. These changes are reversed during cytokinesis. The observed redistribution of Cav1 was reproduced by treatment of interphase cells with nocodazole, suggesting that microtubule rearrangements during mitosis can mediate caveolin relocalization. This study provides new insights into the dynamics of caveolae and highlights precise regulation of caveola budding and recycling during mitosis.

Key words: Caveolae, Caveolin-1, Cavin-1, Cell cycle, Mitosis, Total internal reflection fluorescence

Introduction

Membrane trafficking from and to the plasma membrane is responsible for the transport of many macromolecules and for plasma membrane homeostasis, which is essential during interphase, cellular migration and division (reviewed by Doherty and McMahon, 2009; Scita and Di Fiore, 2010). Caveolae represent an important pathway that links the plasma membrane with intracellular organelles (Echarri et al., 2007; Hansen and Nichols, 2009; Parton and Simons, 2007). Caveolae cycle between the plasma membrane and early endosomes without disassembly of their main protein caveolin-1 (Cav1) (Nichols, 2002; Pelkmans et al., 2004; Pelkmans and Zerial, 2005). Recent work has uncovered a role for membrane trafficking during mitosis (reviewed by Montagnac et al., 2008). For example, clathrin-mediated endocytosis remains constant during all stages of mitosis, but recycling back to the cell surface halts during the rounding-up phase (prophase to metaphase), leading to effective membrane accumulation within the cell and a decrease of plasma membrane surface area (Boucrot and Kirchhausen, 2007). Recycling resumes once the cell enters anaphase and the stored membrane traffics back to the cell surface, where rapid fusion mediates the recovery of plasma membrane area and the subsequent formation of envelopes of the two daughter cells (Boucrot and Kirchhausen, 2007). Caveolae are another important endocytic route, but their dynamics has not been investigated during cell division. In this report, we have used advanced live-cell imaging techniques and quantitative electron microscopy to study caveolae during mitosis. We show that the vast majority of caveolae are dynamic during interphase, with lifetimes ranging from seconds to several minutes. We also reveal an extensive redistribution of caveolae from the plasma membrane to endosomal structures during mitosis. This has profound implications for understanding caveolae dynamics during the important cellular event of division.

Results and Discussion

The majority of caveolae are dynamic

Caveolae were observed by TIRF microscopy and are reported to exist in two pools at the plasma membrane: a majority that is immobile, and a minority displaying a fast 'kiss-and-run' behavior (transient fusion without full collapse of the vesicle) with lifetimes of 2–5 seconds (Pelkmans and Zerial, 2005). By substantial extension of the acquisition period (an image collected every 2 to 10 seconds, for up to 30 minutes) we now report that the majority of caveolae in HeLa or BSC1 cells are not immobile, but instead are endocytosed when observed over periods of several minutes (Fig. 1A and supplementary material Fig. S1A). We noted that the temperature at which the acquisitions were performed had a strong influence on caveola budding. Cooling the cells from 37°C to 30°C was enough to totally block the long-lived (>2 seconds) caveolae in HeLa cells but had little impact on short-lived (≤2 seconds) caveolae (supplementary material Fig. S1B). We note that previous TIRF live-cell imaging studies of caveolae were performed using high imaging frequency (5 Hz) for just a few minutes and not always at 37°C, possibly explaining why the slow, long-lived caveolae were reported as being immobile and non-endocytic (Pelkmans and Zerial, 2005).

Over a period of 10 minutes, the vast majority (85±12%) of Cav1-positive structures were dynamic (Fig. 1B and supplementary material Movie 1). Among the dynamic pool, short-lived caveolae (≤2 seconds) corresponded to 30.8%, whereas the remainder had lifetimes ranging from >2 seconds to over 7 minutes (Fig. 1C). There was no correlation between lifetime and maximum fluorescence intensity reached (supplementary material Fig.

S1C,D), suggesting that the global population of caveolae is more heterogeneous than previously appreciated (Pelkmans and Zerial, 2005). Short-lived caveolae have been shown to be pre-assembled structures displaying a 'kiss-and-run' behavior with the plasma membrane (Pelkmans and Zerial, 2005). To demonstrate that the fast caveolae were fusing with the plasma membrane, an elegant assay taking advantage of pH-sensitive quenching of loaded fluorescently tagged Cholera Toxin B (CTB) was used in a previous study (Pelkmans and Zerial, 2005). We tried to use a similar assay to assess whether the long-lived caveolae were fusing with the plasma membrane. Unfortunately, maintaining the cells at pH 5.5 or 6.2 for periods longer than 1–2 minutes, which is required to follow the dynamics of the long-lived caveolae, induced a significant enlargement of Cav1–EGFP-positive endosomes (results not shown), suggesting a perturbation of Cav1 trafficking and rendering the assay unusable to study the behavior of the long-lived caveolae. Analysis of 500 caveolae imaged fast (5 Hz) showed similar appearance and disappearance kinetics (Fig. 1D and supplementary material Fig. S1E). The vast majority (97±3%) of caveolae that appeared during image acquisition reached their full intensities within 1 second, irrespective of their subsequent lifetime. Similarly, most caveolae (89±7%) disappeared with the same kinetics (Fig. 1D and supplementary material Fig. S1E). Considering that the short-lived caveolae represent less than a third of the dynamic caveolae, we concluded that short-lived and long-lived caveolae arrive at, and depart from, the plasma membrane with similar dynamics. In addition, treatment for 30 minutes with 80 µM dynasore, a cell-permeable small inhibitor of dynamin

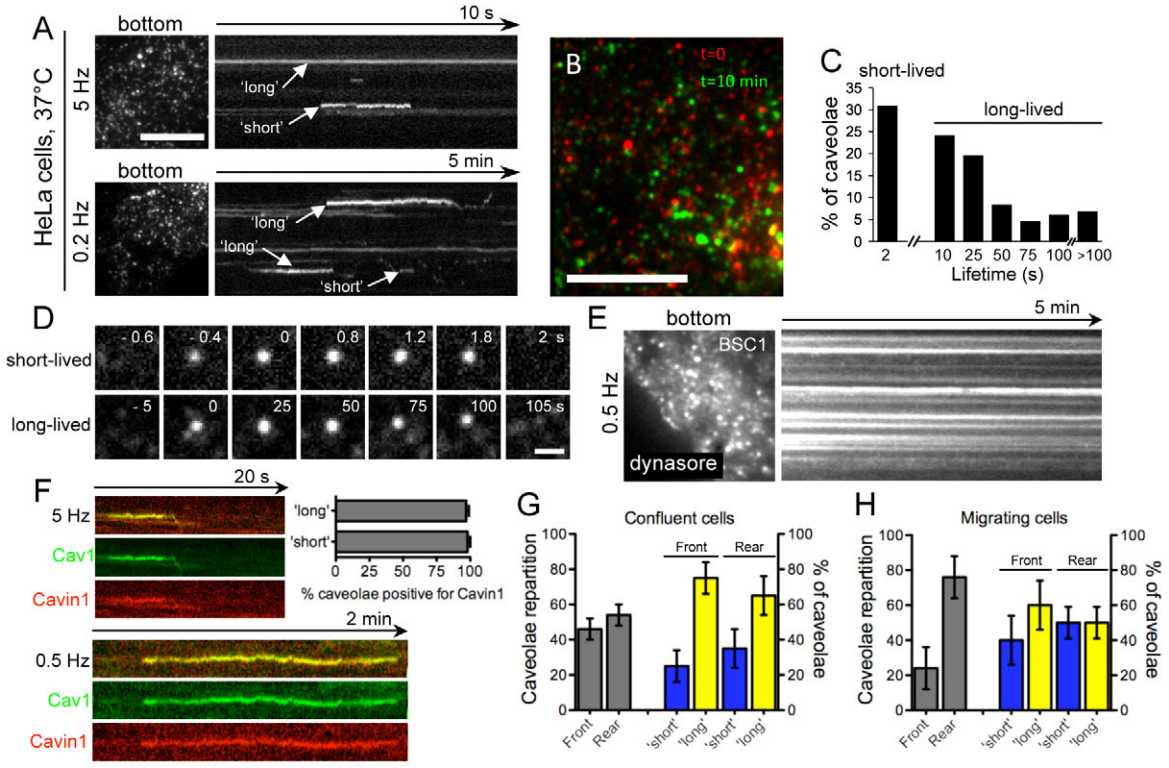

Fig. 1. Slow captures reveal long-lived caveolae during interphase. (**A**) TIRF micrographs of a HeLa cell stably expressing Cav1–EGFP and maintained at 37°C. The still images (labeled 'bottom') correspond to bottom optical section acquired at the beginning of data collection and the kymographs show a projection across time of the complete time series. A representative fast capture (5 Hz, at 200-msecond intervals, for 10 seconds) is displayed in the top panel and a representative slow one (0.2 Hz, at 5-second intervals for 5 minutes) in the lower panel. Note the presence of dynamic caveolae in both fast and slow captures. Scale bar: 10 µm. (**B**) Representative still TIRF images acquired at a 10 minute interval at the plasma membrane of a cell stably expressing Cav1–EGFP. To emphasize the dynamics of most of the caveolae, the first image '*t*=0' was colored red and the last '*t*=10 min' green. Note that very few objects were present in both time points (they appear yellow). The full time series is visible in supplementary material Movie 1. Scale bar: 10 µm. (**C**) Histogram showing distribution of the lifetimes of Cav1–EGFP spots at the plasma membrane calculated from time-series acquired during interphase. The data derive from three cells (*n*=133). (**D**) TIRF time-lapse acquisition of a typical short-lived caveola (acquired at 5 Hz) and of a typical long-lived one (acquired at 0.2 Hz). Scale bar: 5 µm. (**E**) BSC1 cells stably expressing Cav1–EGFP were incubated for 30 minutes with 80 µM dynasore, a cell-permeable small molecule inhibitor of dynamin GTPase function (Macia et al., 2006), before transfer to the TIRF microscope. A time series was collected by TIRF at 0.5 Hz (500 ms interval) for 5 minutes at 37°C. The still image (bottom) corresponds to the lower optical section acquired at the beginning of data collection; the kymograph (right) represents the complete time-series. The data are representative of experiments done in triplicate. Note the numerous frozen Cav1–EGFP structures at the plasma membrane. (**F**) Kymograph showing that short- and long-lived caveolae (imaged at 5 and 0.5 Hz, respectively) contained both Cav1–EGFP and cavin1–RFP. The histogram shows that virtually all Cav1–EGFP-positive caveolae were positive for cavin1–RFP (*n*=50). (**G**) Histogram showing repartition of caveolae on the front or rear of confluent cells (left, gray bars; *n*=200). Note that as BSC-1 cells are poorly polarized when confluent, the rear side was determined as the half surface area of the cell containing the nucleus. Repartition of short-lived (≤2 seconds, blue bars) and long-lived (>2 seconds, yellow bars) caveolae at the front or rear of confluent cells is shown on the right (*n*=200). (**H**) Histogram showing repartition of caveolae on the front or rear of migrating cells (left, gray bars; *n*=200). Cell migration was induced by wounding a confluent monolayer (see Materials and Methods). Cells migrating within the wound 12–16 hours after were imaged. Repartition of short-lived (≤2 seconds, blue bars) and long-lived (>2 seconds, yellow bars) caveolae on the front or rear of confluent cells is shown on the right (*n*=200). Results are mean ± s.e.m.

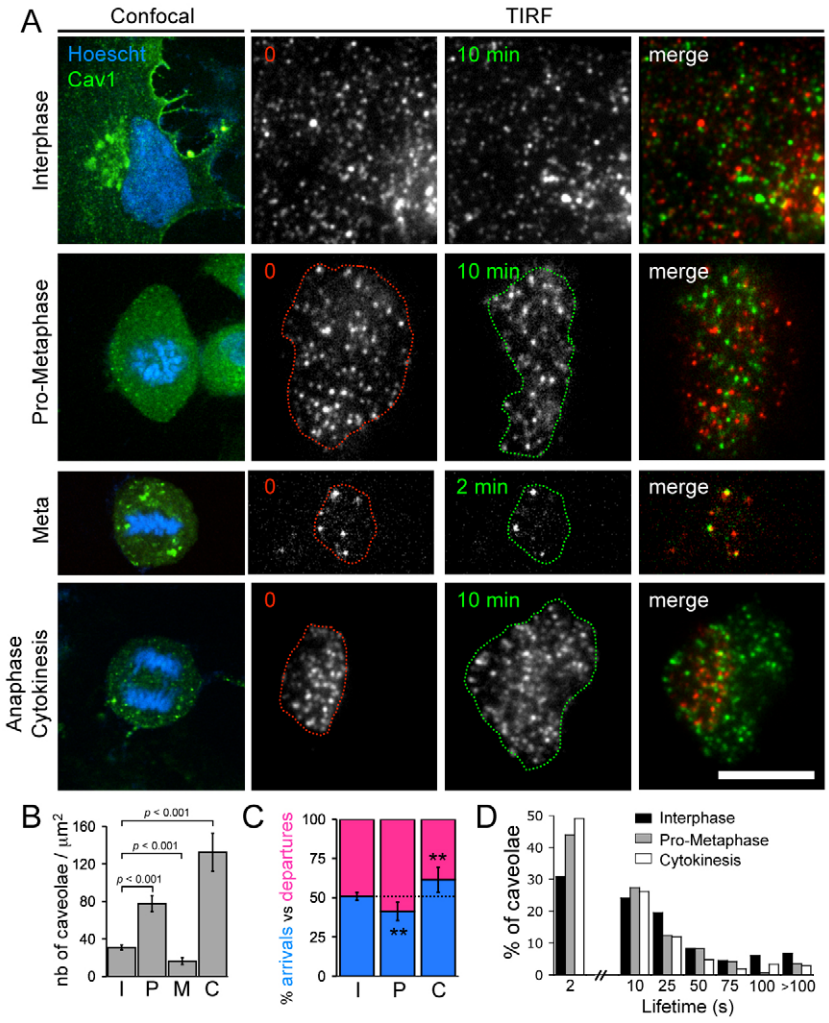

Fig. 2. TIRF analysis of caveolae dynamics along the cell cycle. (**A**) Representative still TIRF images acquired every 10 minutes at the plasma membrane of BSC1 cells stably expressing Cav1–EGFP. The cells were in interphase, rounding-up phase (pro-metaphase), metaphase and membrane recovery phase during daughter cell formation (anaphase–cytokinesis), as illustrated by confocal images on the first column. DNA was stained using the membrane-permeant dye Hoechst 33342. Note also that only one of the two daughter cells was followed in this capture. To emphasize the dynamics of most of the Cav1–EGFP structures during all stages of the cell cycle, the first image '0' was colored in red and the last 10 minutes (2 minutes for metaphase) in green in the overlay panel. To facilitate comparisons, we used here for interphase the same capture than in Fig. 1B. The full time-series of the interphase and cytokinesis cell are visible in supplementary material Movies 1 and 2, respectively. Scale bar: 10 µm. (**B**) Surface density of Cav1–EGFP-containing structures at the plasma membrane during interphase (I), pro-metaphase (P), metaphase (M) and cytokinesis (C). The data (mean ± s.e.m.) were obtained from still images taken every 10 minutes from three time-series for each category. (**C**) Percentages of arrivals (blue) versus departures (pink) of Cav1–EGFP caveolae during interphase (I), pro-metaphase (P) and cytokinesis (C). The data (mean ± s.e.m.) were obtained from six time-series for each category. Note the equilibrium between the arrivals and departures during interphase, but the clear unbalances toward departures or arrivals during pro-metaphase and cytokinesis, respectively. $^{**}P<0.001$. (**D**) The histogram distribution compares lifetimes of Cav1–EGFP spots at the plasma membrane calculated from time-series acquired during interphase (black), pro-metaphase (gray) or cytokinesis (white). The data derive from three cells in interphase (n=133, same data set as used in Fig. 2), four cells in pro-metaphase (n=146) and five cells in cytokinesis (n=210).

(Macia et al., 2006), totally blocked caveolae dynamics at the plasma membrane (Fig. 1E), consistent with the reported dependency of Cav1 endocytosis on dynamin activity (Henley et al., 1998; Oh et al., 1998). Finally, both short- and long-lived caveolae were virtually all positive for polymerase I and transcript release factor (PTRF, also known as and hereafter referred to as cavin-1) (Fig. 1F), a cytoplasmic protein that is associated with mature plasma membrane caveolae (Hill et al., 2008). Altogether these results suggest that 'short-lived' and 'long-lived' caveolae have a similar composition and mechanism of formation.

To investigate whether the repartition between short- and long-lived caveolae varies upon different cellular environments, we investigated the dynamics of these distinct pools of caveolae in confluent versus migrating cells, a state reported to result in the accumulation of caveolae within a specific cellular region (Parat et al., 2003). We first verified that in BSC1 cells, as reported in other cell types (Howes et al., 2010; Parat et al., 2003), caveolae were enriched at the rear of migrating but not confluent cells (Fig. 1G,H, gray bars). We then measured the repartition of short-lived (<2 seconds, blue bars) and long-lived (>2 seconds, yellow bars) caveolae at both the front and rear halves of confluent and migrating cells (Fig. 1G,H). The repartition between short- and long-lived caveolae changed significantly upon cell migration, when both at the front and rear of the cells, the proportion of short-lived caveolae increased (Fig. 1G,H), even though the long-lived caveolae were always the most abundant population. Altogether, our data suggest that the caveolae turnover time, that is the time spent by a caveola on the plasma membrane, varies from a few seconds to several minutes, depending on the particular cellular settings.

Caveola dynamics change during mitosis

We next wondered whether caveolae have the same dynamics during mitosis as in interphase, because recent work highlighted changes in membrane trafficking during cell division (Boucrot and Kirchhausen, 2007). Compared with interphase, the density of caveolae at the plasma membrane increased by a factor of about two when the cell was rounding up during prophase to metaphase (called hereafter pro-metaphase), decreased by a factor of two during metaphase, and increased again by a factor of four as the daughter cells form during anaphase to cytokinesis (called hereafter cytokinesis) (Fig. 2A,B). Such changes in caveolae density suggested variations in turnover time. During interphase, the pool of caveolae at the surface is maintained by a balance between caveolae that arrive and those that depart from the plasma membrane (Fig. 2C). During pro-metaphase, 17±6% more structures were internalized than appeared (Fig. 2C). During cytokinesis, the reverse occurred: 23±8% more caveolae arrived than departed (Fig. 2C and supplementary material Movie 2). During pro-metaphase and cytokinesis, caveolae were more dynamic (i.e. stayed for less time at the plasma membrane and

turned over more often) than during interphase (Fig. 2D, gray and white bars). The average lifetime of 146 caveolae from three cells in pro-metaphase and 210 caveolae from four cells in cytokinesis cells were 17.8 and 15.1 seconds, respectively, around twofold faster than during interphase (30.9 seconds). The short-lived caveolae (≤2 seconds) were more abundant during both phases (43.8% and 49.0%, respectively, compared with 30.8% during interphase), although the majority of structures remained long-lived (Fig. 2D). Altogether, these studies reveal profound changes in the dynamics of caveolae during mitosis.

Cav1 redistributes intracellularly during cell division

The changes in caveola dynamics and variations in caveolae densities during mitosis measured above by TIRF suggested profound modifications in caveolae localization. Global cellular repartition of Cav1 was measured by fast three-dimensional (3D) spinning-disk confocal imaging on live cells naturally undergoing interphase, metaphase or cytokinesis. During interphase, Cav1 is present at the plasma membrane, cytoplasmic vesicles and Golgi complex (Parton and Simons, 2007) (Fig. 3A). Cav1 at the plasma membrane displays a punctate or continuous signal at the sides of

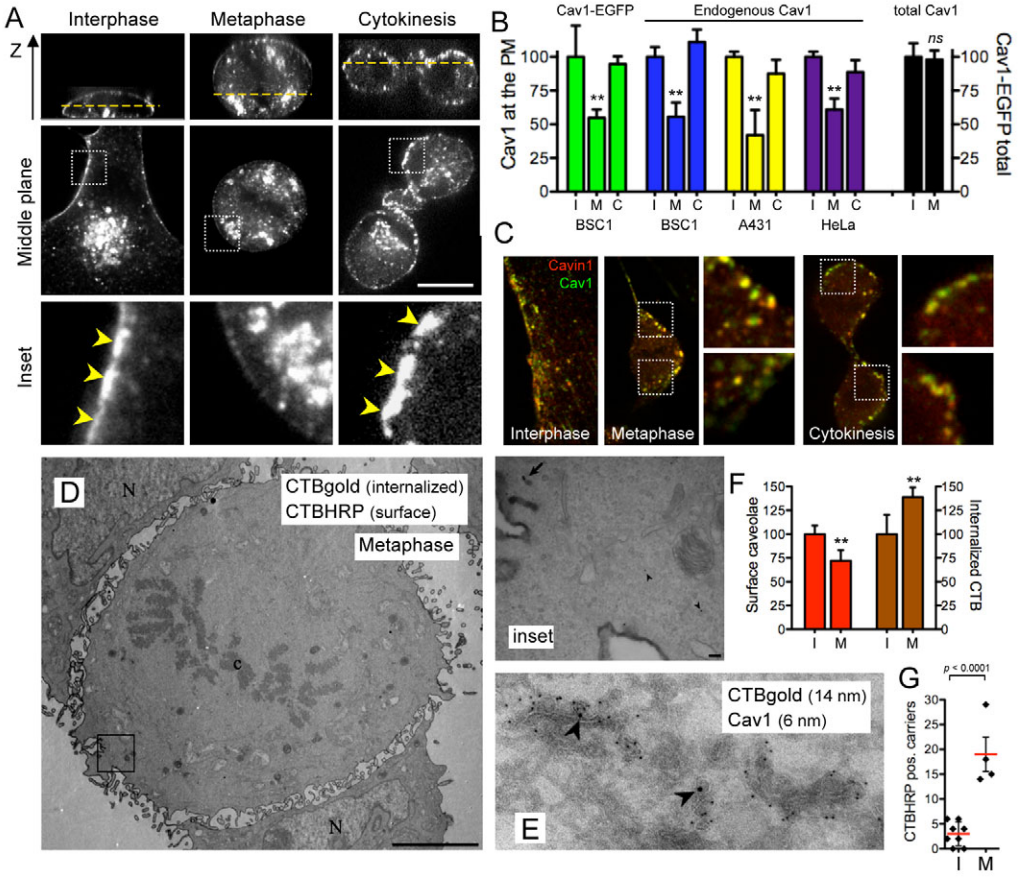

Fig. 3. Cav1 redistributes from the plasma membrane to intracellular compartments during metaphase and returns during cytokinesis. (**A**) Orthogonal fluorescent views corresponding to the distribution of Cav1–EGFP in a live BSC1 cell stably expressing this construct and imaged by spinning-disk confocal microscopy at 37°C. Top panels show the fluorescence signal along the *z*-axis corresponding to sequential optical sections acquired 0.25 µm apart. Middle panels show a single confocal plane positioned within the cell as indicated by the yellow dotted line on the top panels. Insets are focusing on the plasma membrane; arrowheads point to plasma membrane Cav1–EGFP. Scale bar: 10 µm. (**B**) Quantification of Cav1 signals at the plasma membrane (PM) in BSC1 cells stably expressing Cav1–EGFP or in BSC1, A431 and HeLa cells immunolabeled for the endogenous Cav1 (pictures shown in supplementary material Fig. S2G) during interphase (I), metaphase (M) and cytokinesis (C). The PM signals were quantified in every plane of the Z-stacks and normalized to interphase values (mean ± s.e.m.). Total levels of Cav1–EGFP did not vary during metaphase (black bars, right). At least six cells from three independent experiments were analyzed for each category. $^{**}P<0.001$; ns, non-significant. (**C**) Cavin-1–RFP colocalizes with internalized Cav1–EGFP during metaphase. During interphase and cytokinesis cavin-1 colocalizes only with surface Cav1. (**D**) Internalization of CTBgold by metaphase A431 cells. CTBgold was internalized for 20 minutes at 37°C. The cell surface was then labeled with CTBHRP at 4°C. CTBgold that has been internalized is observed within CTBHRP-negative structures (arrowheads); surface CTBgold is associated with CTBHRP-positive structures. Note that CTBgold is frequently observed in internal structures and rarely in surface caveolae. c, chromosomes; N, nucleus. Scale bars: 5 µm (main panel) and 100 nm (inset). (**E**) Immunoelectron microscopy of Cav1 in metaphase A431 cells. CTBgold (14 nm) was internalized for 20 minutes before fixation. Cav1 was specifically labelled using an N-terminally directed antibody that does not recognise the Golgi pool of caveolin (anti-VIPN) (Dupree et al., 1993) and detected with gold-coupled antibody (6 nm). Note the tubular elements labeled for Cav1 (small gold) containing CTBgold (large gold, arrowheads). (**F**) Quantification of surface and internalized caveolae in interphase and metaphase cells. CTBgold internalization using the dual labeling assay, expressed as the ratio of CTBgold within CTBHRP-negative (internal) compartments as a percentage of caveolar and internal gold. Results (n=24 cells) show mean ± s.e.m. $^{**}P<0.001$. (**G**) Caveola budding rate determined by electron microscopy. Cells were incubated with CTBHRP for 1 minute at 37°C, and treated with ascorbic acid to quench the surface CTBHRP peroxidase activity, as described previously (Kirkham et al., 2005; Le Lay et al., 2006). Surface (CTBHRP negative) and internalized caveolae (CTBHRP labeled) are then quantified. The data (mean ± s.e.m.) express the number of caveolae that budded (CTBHRP positive) in a minute as percentage of total plasma membrane caveolae and were obtained from eight cells in interphase and four in metaphase.

adherent cells (Fig. 3A), which correspond to a high density of individual caveola structures (as seen by electron microscopy) (Parton and Simons, 2007). During metaphase, plasma membrane Cav1 levels showed a striking decrease and several large intracellular structures containing Cav1 were observed (Fig. 3A). We verified that these structures were not connected with the plasma membrane, because they failed to stain with the red membrane-impermeant dye FM 4-64 (supplementary material Fig. S2A). Internal Cav1 significantly colocalized with the early endosomal marker EEA1 (supplementary material Fig. S2B), suggesting that Cav1 internalizes during mitosis. Cav1 reappeared at the cell surface during cytokinesis (Fig. 3A). Whole caveolae are probably internalized during mitosis because not only Cav1, but also cavin-1, a recently identified constituent of caveolae (Hill et al., 2008), displayed similar relocalization (Fig. 3C). Two lines of evidence suggested that caveolae redistribute by membrane trafficking during mitosis. First, treatment for 30 minutes with 80 μM dynasore, which blocked Cav1 dynamics during interphase (Fig. 1E), also inhibited the decrease of Cav1 levels at the plasma membrane of pro-metaphase cells (supplementary material Fig. S2C). Second, treatment with the Golgi-dispersing drug Brefeldin A (BFA) did not perturb the reappearance of Cav1 during cytokinesis (supplementary material Fig. S2D), showing that reappearance of Cav1 at the cell surface results from the fusion of the previously stored structures with the plasma membrane, rather than from a newly synthesized pool. Time-lapse spinning-disk confocal microscopy performed on a middle section plane of dividing cells illustrated the disappearance of the plasma-membrane-localized Cav1 during the rounding-up phase and its reappearance as the two daughter cells form (supplementary material Fig. S2E,F and Movie 3). The specific redistribution of Cav1 during metaphase was also observed for endogenous Cav1 in BSC1, A431 and HeLa cells. Cav1 subsequently returned to the plasma membrane during cytokinesis (Fig. 3B and supplementary material Fig. S2H).

We next used quantitative electron microscopy to examine the distribution of Cav1 and caveolae in mitotic cells. Immunogold labeling for Cav1 using an N-terminal antibody, which exclusively labels the cell surface caveolae of interphase cells (Dupree et al., 1993), showed strong labeling on cytoplasmic vesicles (including structures with caveola morphology) and tubules of pro-metaphase cells (Fig. 3D,E and supplementary material Fig. S3), confirming the internalization of Cav1 during the mitotic round up. Internalized Cholera Toxin B coupled to horseradish peroxidase (CTBHRP), a non-specific surface marker, labeled tubulovesicular endocytic structures, but strikingly also labeled numerous structures with the morphology of budded caveolae (Fig. 3D and supplementary material Fig. S3A–D). Gold-labeled CTB (CTBgold), which in contrast to CTBHRP is highly concentrated in caveolae (Parton et al., 1994) (see also supplementary material Fig. S3E), was used in a dual-labeling strategy (Parton et al., 1994) with CTBgold as internalized caveolar marker, and subsequently CTBHRP at 4°C as surface marker (Fig. 3D). This confirmed the intracellular redistribution of Cav1 during metaphase. Compared with interphase cells, pro-metaphase cells showed a decrease in morphologically distinguishable caveolae at the cell surface and an increase in internalized CTBgold-positive, CTBHRP-negative structures (Fig. 3D,F). Quantification of surface caveolae in metaphase showed a decrease of 28±11% ($P<0.001$) compared with interphase cells (Fig. 3F). Conversely, the percentage of internalized caveolae increased by 49±10% ($P<0.0001$) in metaphase compared with interphase cells (Fig. 3F). To confirm the change in caveola dynamics during mitosis reported in Fig. 2, the number of caveolae that budded in 1 minute at 37°C as a percentage of total plasma membrane caveolae was quantified. We used a recently developed method that relies on the quenching of the activity of surface CTBHRP by ascorbic acid and recognition of budded caveolae by their characteristic size and morphology (Kirkham et al., 2005; Le Lay et al., 2006). In interphase cells, an average of 3±2% of the total caveolae budded in 1 minute (Fig. 3G). At this rate, the whole plasma membrane pool of Cav1 will be turned over within ~20–30 minutes, consistent with the kinetics reported above. In pro-metaphase cells, 19±7% of the total caveolae budded in a minute (Fig. 3G), which corresponded to a ~sixfold increase of caveolae dynamics. Collectively, our results show that caveolae redistribute intracellularly during metaphase to return at the surface during cytokinesis. These fluxes are mediated by an activation of caveola dynamics, resulting in increased trafficking of these organelles during cell division.

Microtubule depolymerization in interphase mimics mitotic redistribution of caveolae

To identify possible mechanisms involved in the transient redistribution of caveolae during metaphase, we next investigated the involvement of the microtubule cytoskeleton. Mitosis is associated with profound cytoskeletal rearrangements mediating the proper separation of the chromosomes pairs. In particular, microtubules depolymerize to reassemble the mitotic spindle in an organized array (Goshima and Scholey, 2010). Because recent work linked microtubule dynamics to plasma membrane targeting of caveolae during interphase (Wickstrom et al., 2010), we wondered whether microtubule depolymerization during cell division could mediate caveolae redistribution. Microtubule perturbation could not be investigated during mitosis because it blocks proper cell division (Zieve, 1984). However, upon treatment of interphase BSC1 cells with the microtubule-depolymerizing drug nocodazole, levels of Cav1 decreased significantly at the plasma membrane and redistributed in part to early endosomes labeled with EEA1 (Fig. 4A–C), which occurs naturally during prophase to metaphase (Fig. 3). Washout of the drug (and subsequent repolymerization of microtubules) caused a significant shift of Cav1 back to the cell surface (Fig. 4A–C). As observed during the prophase to metaphase transition, the progressive departure of Cav1 from the plasma membrane in nocodazole-treated cells was due to a reduction of the number of caveolae that arrive at the plasma membrane (Fig. 4D). During washout of the drug, the number of caveolae that arrived at the plasma membrane increased beyond the number that departed, mediating the progressive restoration of the caveolae pool (Fig. 4D). Because microtubule depolymerization during interphase was enough to induce a similar redistribution to that observed during mitosis, we conclude that natural microtubule rearrangements during cell division can mediate changes in caveola localization, perhaps by trapping caveolae intracellularly and thus decreasing the number of caveolae that can recycle from internal stores to the plasma membrane.

Conclusions

This study revealed that the vast majority of caveolae are dynamic. In addition to the short-lived (~2–5 seconds) caveolae previously described (Pelkmans and Zerial, 2005), we observed that a large proportion of the caveolae previously described as immobile are in

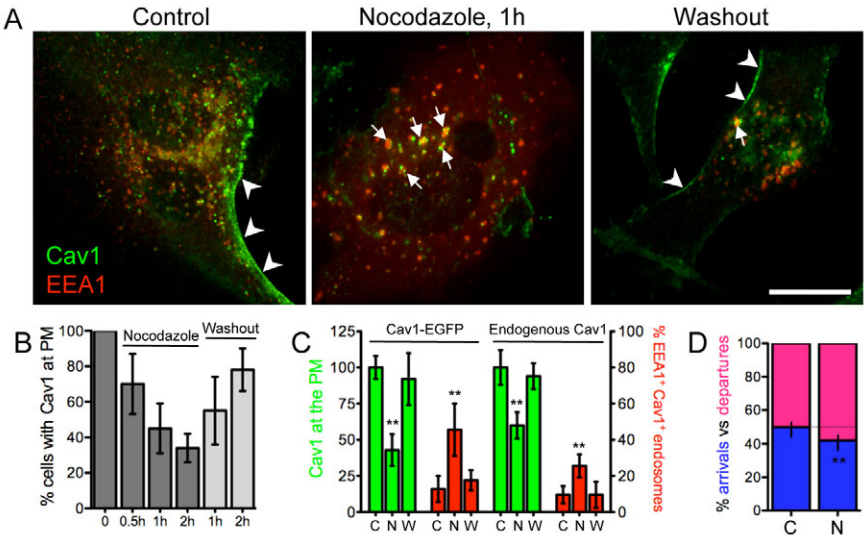

Fig. 4. Microtubule depolymerization induces relocalization of surface caveolae to early endosomes. (**A**) BSC1 cells stably expressing Cav1–EGFP and transiently expressing EEA1-mRFP were incubated at 37°C with normal medium (control) or with 10 µM nocodazole (a microtubule depolymerizing drug) for 1 hour (Nocodazole, 1 hour), or with 10 µm noccodazole for 1 hour followed by 1 hour in normal medium (Washout). A representative middle confocal plane is presented. Arrowheads indicate plasma membrane Cav1, arrows show internalized Cav1–EGFP colocalizing with EEA1–mRFP. Scale bar: 10 µm. (**B**) Percentage of cells having Cav1 at the plasma membrane before (0) and after 0.5, 1 or 2 hours incubation with 10 µM nocodazole (Nocodazole, dark grey bars), followed by 1 or 2 hours incubation back to normal medium (Washout, light grey bars).The data (mean ± s.e.m.) were obtained from at least 100 cells (from three independent experiments) at each time point. (**C**) Green bars show quantification of Cav1 signals at the plasma membrane in BSC1 cells stably expressing Cav1–EGFP (left), or fixed and stained for endogenous Cav1 (right) and treated as in A for 1 hour at 37°C with control (C), 10 µM nocodazole (N) or 10 µM nocodazole for 1 hour followed by a 1 hour washout with normal medium (W). The plasma membrane signals were quantified in each plane of Z-stacks and normalized to interphase values (mean ± s.e.m.). Red bars show percentage of EEA1-positive early endosomes colocalizing with Cav1–EGFP in cells treated the same way. Ten cells from three independent experiments were analyzed for each category. $^{**}P<0.001$. (**D**) Percentages of arrivals (blue) versus departures (pink) of Cav1–EGFP caveolae in cells treated as in A for 1 hour at 37°C with control (C), 10 µM nocodazole (N). The data (mean ± s.e.m.) were obtained from two time-series for each category. $^{**}P<0.001$.

fact long-lived (10 seconds to over 7 minutes). Endocytosis of the long-lived structures was only observed in cells strictly kept at 37°C. At 30°C, only the short-live caveolae were observable, the rest being seemingly static. Long-lived caveolae all appeared and disappeared with similar rates as the equivalent steps of the short-lived ones, but because many individual fluorescence traces of long-lived caveolae showed significant intensity variations (not shown), it suggests that some might be multi-caveolae assemblies, potentially formed by several individual caveolar vesicles docking on top of each other, as observed previously by electron microscopy (Parton et al., 1994).

The extensive trafficking (internalization, followed by reappearance at the surface) of most caveolae during cell division reported here uncovers a mitosis-specific redistribution of Cav1. A decrease in caveolae arrivals coupled to consistent budding results in an imbalance between arrivals versus departures (Fig. 2), and a progressive net decrease of surface caveolae (Fig. 3). What could be the function of such trafficking? One hypothesis is that it could contribute to the variations of the plasma membrane area during cell division that we have previously reported (Boucrot and Kirchhausen, 2007). However, considering the predicted low capacity of membrane uptake by caveolae endocytosis (Parton et al., 1994; Parton and Simons, 2007), it is unlikely to be a major membrane uptake pathway, consistent with the viability of *Cav1*$^{-/-}$ mice and the ability of *Cav1*$^{-/-}$ cells to divide. Nevertheless, the importance of Cav1 in the fine regulation of the cell cycle has been revealed by detailed studies of *Cav1*-null cells or cells overexpressing Cav1–GFP (Cerezo et al., 2009; Fang et al., 2007; Galbiati et al., 2001). These studies link Cav1 to Rac1- and p53/p21-dependent pathways, which regulate of the progression through the G1 phase of the cell cycle. In addition, Del Pozo and colleagues have implicated caveolin internalization in this process (Cerezo et al., 2009). Thus, the precise and regulated redistribution of Cav1 during mitosis reported here might be required for proper progression through the subsequent G1 phase.

Internalization of caveolae during mitosis could be required for the correct distribution of Cav1 between the two daughter cells. The localization of Cav1 at the plasma membrane of many interphase cells is highly asymmetrical and polarized, especially during cell migration (Lentini et al., 2008; Parat et al., 2003). If the distribution of Cav1 between the two daughter cells is not equal, one cell would inherit an excess of Cav1. This would result in the same consequences as Cav1 overexpression, which is known to inhibit cell proliferation by blocking the progression through G1 (Fang et al., 2007; Galbiati et al., 2001). Therefore, redistribution of Cav1 to intracellular endosomal structures, which partition stochastically during mitosis (Bergeland et al., 2001), might ensure the equal distribution of Cav1 between the two daughter cells. Use of specific inhibitors of caveola endocytosis will be required to pinpoint the precise role of the changes in caveola dynamics revealed here in Cav1-mediated regulation of the cell cycle.

The precise mechanisms inducing Cav1 redistribution during mitosis are yet to be elucidated, but this study provides some potential new clues. Our results suggest that microtubule depolymerization and reorganization, which occurs during prophase and metaphase, could explain, at least in part, caveolae

redistribution because microtubule depolymerization in interphase cells was enough to induce a similar change (Fig. 4). In both cases, a decrease in the rate of arrivals of caveolae to the surface coupled to a sustained budding induced the net decrease in the surface pool. A microtubule-based transport has been recently shown to mediate traffic of caveolae to the cell surface (Wickstrom et al., 2010). Mitosis provides a natural state of activated and directed trafficking of caveolae and thus future studies during this stage of the cell cycle might also be useful to elucidate molecular mechanisms of caveolae trafficking.

Materials and Methods

Cells, plasmids and reagents

Monkey kidney epithelial cells BSC-1 (ATCC CCL-26, referred to here as 'BSC1') and human HeLa (ATCC CCL-2) and A-431 (ATCC CRL 1555, referred to here as 'A431') cells were grown as adherent cells in DMEM supplemented with 10% fetal bovine serum (FBS). We have generated a HeLa and a BSC1 cell line stably expressing an EGFP-fusion chimeras of Cav1 (Cav1–EGFP) by transfecting the plasmid using FuGene 6 (Roche Diagnotics) or Lipofectamine 2000 (Invitrogen), respectively, followed by selection and maintenance with complete medium supplemented with geneticin (G418, 0.5–0.7 mg/ml). Transient transfections of cavin-1–mRFP and EEA1–mRFP were performed on the Cav1–EGFP stable BSC1 cell line using Lipofectamine 2000. Cells were imaged 24–48 hours later.

The cells were not synchronized by any chemical means. The stage along the cell cycle was determined in the population of asynchronous cells using phase-contrast bright-field illumination according to the following criteria: cells in prophase contain condensed chromosomes surrounded by the nuclear envelope; cells in metaphase appear round, lack their nuclear envelope and display condensed chromosomes aligned at the metaphase plate; cells undergoing cytokinesis (but before abscission) display a deep furrow, still have condensed chromosomes and start to show their nuclear envelope.

The following antibodies were used: rabbit anti-Cav1, anti-VIPN (Dupree et al., 1993) and RbTL C13630 (BD Transduction Laboratory). The following reagents were used: human transferrin–HRP (Rockland Inc), CTBHRP (Sigma), nocodazole (Sigma), Hoechst 33342 (Sigma) and dynasore (Macia et al., 2006). CTBgold was prepared as described previously (Parton, 1994) and each batch of CTBgold was tested for specificity for labeling of surface caveolae at 4°C as described previously (Parton, 1994).

Quantitative electron and immunoelectron microscopy

Cav1 immunolabeling was performed with the anti-VIPN, anti-Cav1 antibody raised against the N-terminus of canine Cav1 that does not recognize the Golgi pool of caveolin (Dupree et al., 1993). For internalization experiments two different schemes were used based on previously described methods (Parton et al., 1994). CTBgold (14 nm) was bound to the cell surface at 4°C with or without 10 μg/ml transferrin–HRP and internalized for 20 minutes at 37°C before surface labeling with CTBHRP at 4°C (Parton, 1994). In other experiments, CTBHRP was bound to the cell surface at 4°C for 30 minutes and the cells were warmed at 37°C for 20 minutes before fixation. For quantification of caveola dynamics in A431 cells using the DAB and ascorbic acid method, experiments were performed and quantified exactly as described previously (Kirkham et al., 2005). Budded caveolae were defined by their content of DAB reaction product and morphology, as in previous studies (Le Lay et al., 2006). Metaphase cells were identified by their characteristic morphological appearance under the light microscope, marked, and then ultrathin sections of the same areas, cut parallel to the culture substratum, were prepared. No synchronization protocol was used and only cells that could be unequivocally identified as being in metaphase were further analyzed. Interphase cells in the same dishes were analyzed in the same manner.

Fluorescence microscopy acquisitions

Cells grown on No. 1.5 glass coverslips (25 μm in diameter) were washed with DMEM supplemented with 10% FBS and put in imaging buffer (α-MEM without Phenol Red supplemented with 20 μm HEPES, pH 7.4 and 5 % FBS). The coverslips were transferred to a sample holder (20/20 Technology, Inc., Wilmington, NC) and kept on the microscope at 37°C with 5% CO_2 and 100% humidity located inside an environmental chamber set at 37°C also containing the objective lenses. In some experiments, dynasore (80 μM in 0.4 % DMSO final) was directly dissolved in PBS supplemented with 0.1 μm $CaCl_2$, 1 μm $MgCl_2$, glucose (4.5 g/l) and 1% Nu-Serum (BD Biosciences). The cells were washed three times with pre-warmed PBS-supplemented solution (without dynasore) before addition of dynasore-containing medium to the cell for 30 minutes at 37°C before imaging in the same medium (with dynasore).

Live-cell time series or 3D imaging were done using a spinning disk confocal head (Perkin Elmer, Boston, MA) coupled to a fully motorized inverted microscope (Axiovert 200M, Carl Zeiss) equipped with a 63× oil-immersion lens (Pan Apochromat, 1.4 NA, Carl Zeiss). A 50 mW solid-state laser (473 nm; Crystal Laser) coupled to the spinning head through an acoustic-optical tuneable filter (AOTF) was used as light source. The imaging system operates under control of SlideBook 4.2 (Intelligent Imaging Innovations) and includes a computer-controlled spherical aberration correction device (SAC, Intelligent Imaging Innovations) installed between the objective lens and the back illuminated 16-bit CCD camera (Cascade 512B; Roper Scientific, Photometrics) used with a binning of 1×1. Rapid acquisition of sequential optical sections spaced 0.25 μm apart was achieved with the aid of a piezo-driven stage (Applied Scientific Instrumentation). To reduce photo-bleaching, the illumination was turned off during the readout period from the CCD to the computer.

TIRF experiments were performed using an inverted microscope (Axiovert 200M; Carl Zeiss) equipped with a Zeiss TIRF module, a 100× 1.45 NA Zeiss TIRF oil-immersion lens and computer-controlled SAC. Cells were kept on the microscope at 37°C with 5% CO_2 and 100% humidity located inside an environmental chamber set at 37°C also containing the objective lens. A 470 nm solid-state laser (Crystal lasers, Reno, NV) was the source of illumination in TIRF. A back-illuminated Cascade 512B (Roper Scientific) was used for image acquisition under no-gain magnification mode. To reduce photo-bleaching, the illumination was turned off during the readout period from the CCD to the computer.

Fluorescence imaging of fixed cells was done with an upright microscope (Carl Zeiss) equipped with manually-driven SAC and a 40× or 63× 1.4 NA oil-immersion Zeiss objective lenses. Epifluorescence illumination was provided through Lambda DG-4 illumination unit (Sutter Instruments). 12-bit digital images were obtained with a 12-bit cool CCD camera (Cool Snap HQ, Photometrics) with 2×2 binning. Images were acquired with exposure times between 100 and 500 milliseconds. Three-dimensional stacks of sequential optical sections were acquired 0.3 μm apart. No deconvolution was applied on any images shown in the figures.

Particle tracking and analysis

The following sequential steps were used to automatically identify and track Cav1–EGFP clusters in TIRF captures: (1) Creation of a mask for every cluster. A no-neighbor deconvolution was applied to each raw image (using Slidebook 4.2), to increase the signal-to-noise ratio and to even out the signal fluctuations in the background. The deconvolved images were then smoothed by applying a Gaussian spatial two-dimensional radial transformation (radius=1 pixel) and fast spatial changes in signal were eliminated by applying a Laplacian two-dimensional derivative. Finally, a mask corresponding to each spot in the images was obtained by 'AND' logical operation applied between the images resulting from the Laplacian transformation and the deconvolved images segmented by intensity. (2) Particle identification: determination of the spatial coordinates for all the centroids of every masked spot in any given image. (3) Particle tracking: the masked spots were connected in time, by allowing the software (Slidebook 4.2) to explore the position of every spot along the time series. All particles tracked were individually validated. Every dynamic spot was accepted, as far as they were individual objects (diffraction-limited) and all their 'history' can be known (from appearance to disappearance). The relative fluorescence intensity of each spot masked in the raw image corresponds to the difference in fluorescence signal intensity defined by the mask minus the average background signal of the cytosol. Calculation of several descriptors (lifetime, maximal intensity, density, etc.) was performed using Slidebook 4.2. Most caveolae appeared and disappeared without *x*-*y* movements. For the caveolae that were moving in *x*-*y* for few frames while they appeared or disappeared, only the stationary phase at the plasma membrane was used for calculation. To determine the ratio between arrivals versus departures of caveolae, all objects appearing or disappearing during the course of the time-series were separately counted. Statistical significances (*P* values) were calculated by unpaired two-tailed Student's *t*-test. *P* values less than 0.05 were considered significant.

We are grateful to Brigitte Joggerst, Nicole Schieber (R.G.P.) and Saveez Saffarian (E.B.) for technical assistance. R.G.P. made the initial observation and performed and analysed the electron microscopy experiments together with M.T.H. All the other experiments were performed and analyzed by E.B. The project was designed and supervised by R.G.P. and T.K. The paper was written by E.B. and R.G.P. with input from all the other authors. This work was supported by grants from the National Health and Medical Research Council of Australia (R.G.P.), the Human Frontier Science Program (R.G.P.) and the US National Institutes of Health grants GM 075252 and GM 62566 (T.K.). E.B. was a long-term fellow of the International Human Frontier Science Program Organization (HFSP). The authors acknowledge the use of facilities in the Australian Microscopy and Microanalysis Facility (AMMRF) at the Centre for Microscopy and Microanalysis at The University of Queensland. Deposited in PMC for release after 12 months.

Supplementary material available online at
http://jcs.biologists.org/cgi/content/full/124/12/1965/DC1

References

Bergeland, T., Widerberg, J., Bakke, O. and Nordeng, T. W. (2001). Mitotic partitioning of endosomes and lysosomes. *Curr. Biol.* **11**, 644-651.

Boucrot, E. and Kirchhausen, T. (2007). Endosomal recycling controls plasma membrane area during mitosis. *Proc. Natl. Acad. Sci. USA* **104**, 7939-7944.

Cerezo, A., Guadamillas, M. C., Goetz, J. G., Sanchez-Perales, S., Klein, E., Assoian, R. K. and Del Pozo, M. A. (2009). Absence of Caveolin-1 increases proliferation and Anchorage-independent growth by a Rac-dependent, Erk-independent mechanism. *Mol. Cell. Biol.* **29**, 5046-5059.

Doherty, G. J. and McMahon, H. T. (2009). Mechanisms of endocytosis. *Annu. Rev. Biochem.* **78**, 857-902.

Dupree, P., Parton, R. G., Raposo, G., Kurzchalia, T. V. and Simons, K. (1993). Caveolae and sorting in the trans-Golgi network of epithelial cells. *EMBO J.* **12**, 1597-1605.

Echarri, A., Muriel, O. and Del Pozo, M. A. (2007). Intracellular trafficking of raft/caveolae domains: insights from integrin signaling. *Semin. Cell Dev. Biol.* **18**, 627-637.

Fang, K., Fu, W., Beardsley, A. R., Sun, X., Lisanti, M. P. and Liu, J. (2007). Overexpression of caveolin-1 inhibits endothelial cell proliferation by arresting the cell cycle at G0/G1 phase. *Cell Cycle* **6**, 199-204.

Galbiati, F., Volonte, D., Liu, J., Capozza, F., Frank, P. G., Zhu, L., Pestell, R. G. and Lisanti, M. P. (2001). Caveolin-1 expression negatively regulates cell cycle progression by inducing G(0)/G(1) arrest via a p53/p21(WAF1/Cip1)-dependent mechanism. *Mol. Biol. Cell* **12**, 2229-2244.

Goshima, G. and Scholey, J. M. (2010). Control of mitotic spindle length. *Annu. Rev. Cell Dev. Biol.* **26**, 21-57.

Hansen, C. G. and Nichols, B. J. (2009). Molecular mechanisms of clathrin-independent endocytosis. *J. Cell Sci.* **122**, 1713-1721.

Henley, J. R., Krueger, E. W., Oswald, B. J. and McNiven, M. A. (1998). Dynamin-mediated internalization of caveolae. *J. Cell Biol.* **141**, 85-99.

Hill, M. M., Bastiani, M., Luetterforst, R., Kirkham, M., Kirkham, A., Nixon, S. J., Walser, P., Abankwa, D., Oorschot, V. M., Martin, S. et al. (2008). PTRF-Cavin, a conserved cytoplasmic protein required for caveola formation and function. *Cell* **132**, 113-124.

Howes, M. T., Kirkham, M., Riches, J., Cortese, K., Walser, P. J., Simpson, F., Hill, M. M., Jones, A., Lundmark, R., Lindsay, M. R. et al. (2010). Clathrin-independent carriers form a high capacity endocytic sorting system at the leading edge of migrating cells. *J. Cell Biol.* **190**, 675-691.

Kirkham, M., Fujita, A., Chadda, R., Nixon, S. J., Kurzchalia, T. V., Sharma, D. K., Pagano, R. E., Hancock, J. F., Mayor, S. and Parton, R. G. (2005). Ultrastructural identification of uncoated caveolin-independent early endocytic vehicles. *J. Cell Biol.* **168**, 465-476.

Le Lay, S., Hajduch, E., Lindsay, M. R., Le Liepvre, X., Thiele, C., Ferre, P., Parton, R. G., Kurzchalia, T., Simons, K. and Dugail, I. (2006). Cholesterol-induced caveolin targeting to lipid droplets in adipocytes: a role for caveolar endocytosis. *Traffic* **7**, 549-561.

Lentini, D., Guzzi, F., Pimpinelli, F., Zaninetti, R., Cassetti, A., Coco, S., Maggi, R. and Parenti, M. (2008). Polarization of caveolins and caveolae during migration of immortalized neurons. *J. Neurochem.* **104**, 514-523.

Macia, E., Ehrlich, M., Massol, R., Boucrot, E., Brunner, C. and Kirchhausen, T. (2006). Dynasore, a cell-permeable inhibitor of dynamin. *Dev. Cell* **10**, 839-850.

Montagnac, G., Echard, A. and Chavrier, P. (2008). Endocytic traffic in animal cell cytokinesis. *Curr. Opin. Cell Biol.* **20**, 454-461.

Nichols, B. J. (2002). A distinct class of endosome mediates clathrin-independent endocytosis to the Golgi complex. *Nat. Cell Biol.* **4**, 374-378.

Oh, P., McIntosh, D. P. and Schnitzer, J. E. (1998). Dynamin at the neck of caveolae mediates their budding to form transport vesicles by GTP-driven fission from the plasma membrane of endothelium. *J. Cell Biol.* **141**, 101-114.

Parat, M. O., Anand-Apte, B. and Fox, P. L. (2003). Differential caveolin-1 polarization in endothelial cells during migration in two and three dimensions. *Mol. Biol. Cell* **14**, 3156-3168.

Parton, R. G. (1994). Ultrastructural localization of gangliosides; GM1 is concentrated in caveolae. *J. Histochem. Cytochem.* **42**, 155-166.

Parton, R. G. and Simons, K. (2007). The multiple faces of caveolae. *Nat. Rev. Mol. Cell Biol.* **8**, 185-194.

Parton, R. G., Joggerst, B. and Simons, K. (1994). Regulated internalization of caveolae. *J. Cell Biol.* **127**, 1199-1215.

Pelkmans, L. and Zerial, M. (2005). Kinase-regulated quantal assemblies and kiss-and-run recycling of caveolae. *Nature* **436**, 128-133.

Pelkmans, L., Burli, T., Zerial, M. and Helenius, A. (2004). Caveolin-stabilized membrane domains as multifunctional transport and sorting devices in endocytic membrane traffic. *Cell* **118**, 767-780.

Scita, G. and Di Fiore, P. P. (2010). The endocytic matrix. *Nature* **463**, 464-473.

Wickstrom, S. A., Lange, A., Hess, M. W., Polleux, J., Spatz, J. P., Kruger, M., Pfaller, K., Lambacher, A., Bloch, W., Mann, M. et al. (2010). Integrin-linked kinase controls microtubule dynamics required for plasma membrane targeting of caveolae. *Dev. Cell* **19**, 574-588.

Zieve, G. W. (1984). Nocodazole and cytochalasin D induce tetraploidy in mammalian cells. *Am. J. Physiol.* **246**, C154-C156.

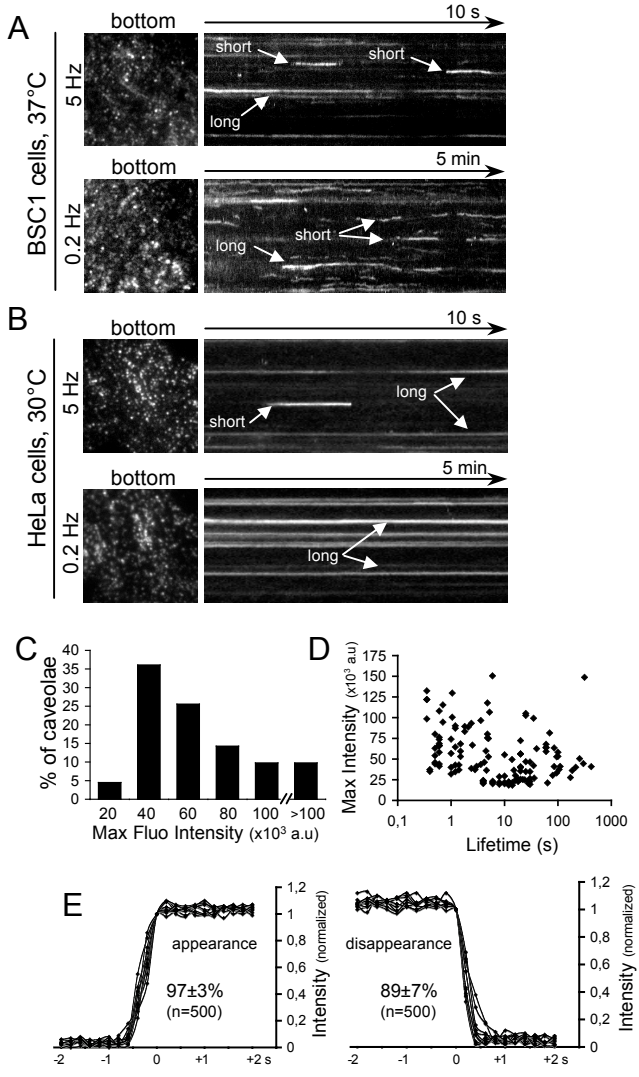
A
bottom
10 s
short
short
long
BSC1 cells, 37°C
5 Hz
bottom
5 min
long
short
0.2 Hz
B
bottom
10 s
long
short
HeLa cells, 30°C
5 Hz
bottom
5 min
long
0.2 Hz
C
% of caveolae
Max Fluo Intensity (x10³ a.u)
D
Max Intensity (x10³ a.u)
Lifetime (s)
E
appearance
97±3%
(n=500)
disappearance
89±7%
(n=500)
Intensity (normalized)

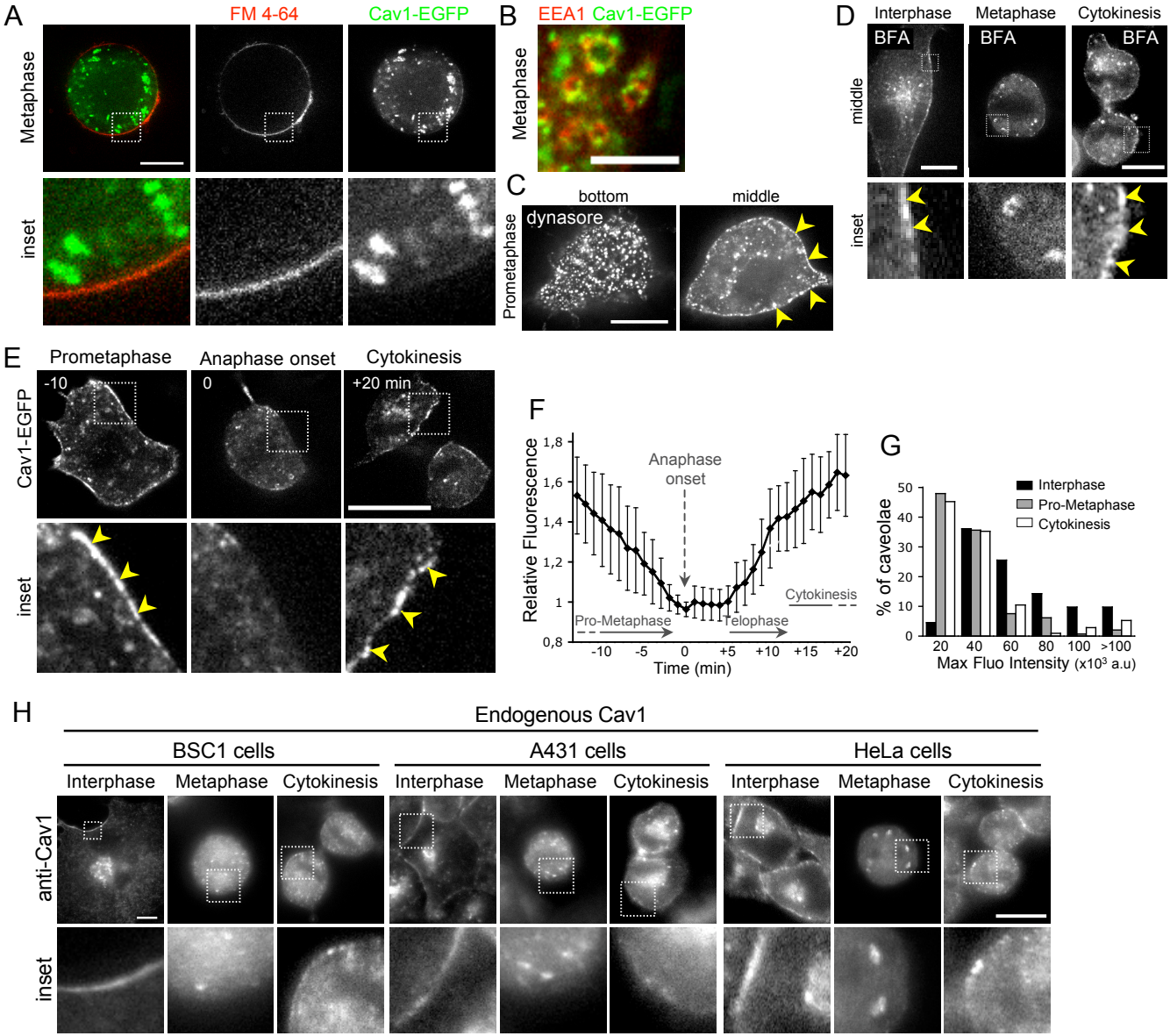
A
FM 4-64
Cav1-EGFP
Metaphase
inset
B
EEA1 Cav1-EGFP
Metaphase
C
bottom
middle
dynasore
Prometaphase
D
Interphase
Metaphase
Cytokinesis
BFA
middle
inset
E
Prometaphase
Anaphase onset
Cytokinesis
Cav1-EGFP
-10
0
+20 min
inset
F
Relative Fluorescence
Anaphase onset
Pro-Metaphase
Telophase
Cytokinesis
Time (min)
G
% of caveolae
Interphase
Pro-Metaphase
Cytokinesis
Max Fluo Intensity (x10³ a.u)
H
Endogenous Cav1
BSC1 cells
A431 cells
HeLa cells
Interphase
Metaphase
Cytokinesis
anti-Cav1
inset

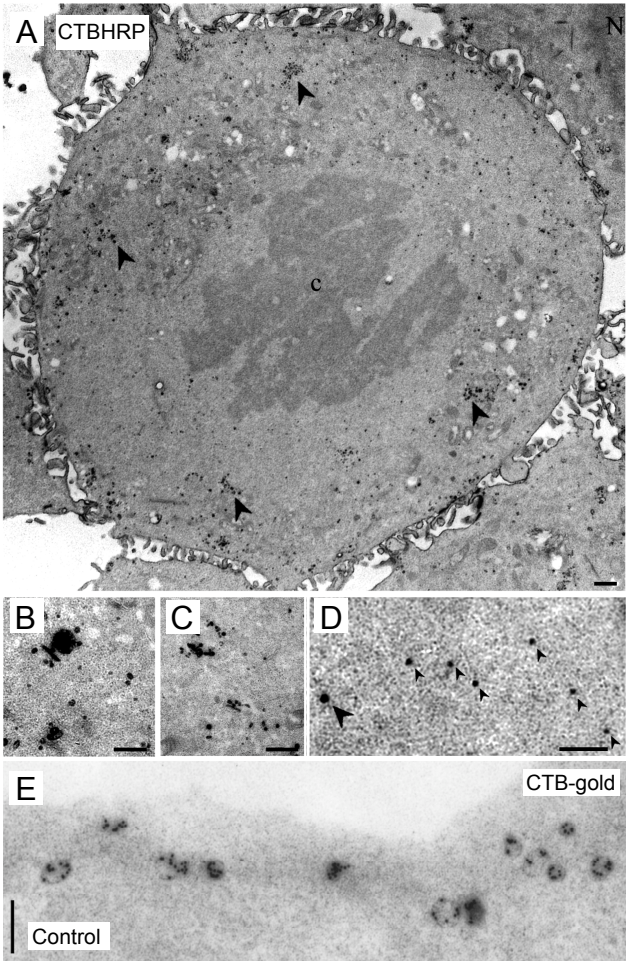
A
CTBHRP
N
c
B
C
D
E
CTB-gold
Control